

Article

An Experimental Investigation on the Pool Boiling Heat Transfer of R-134a on Microporous Cu-MWCNT Composite Surfaces

Ajay D. Pingale ^{1,*}, Anil S. Katarkar ², Mahadev Madgule ¹, Swapan Bhaumik ² and Sachin U. Belgamwar ³

¹ Department of Mechanical Engineering, Pimpri Chinchwad College of Engineering, Pune 411044, India; mahadev.madgule@gmail.com

² Department of Mechanical Engineering, National Institute of Technology Agartala, Agartala 799046, India; anil.katarkar@gmail.com (A.S.K.); drsbhaumik@gmail.com (S.B.)

³ Department of Mechanical Engineering, Birla Institute of Technology and Science Pilani, Pilani 333031, India; sachinbelgamwar@pilani.bits-pilani.ac.in

* Correspondence: ajay9028@gmail.com; Tel.: +91-99-7059-8292

Abstract: Multiwalled carbon nanotubes (MWCNTs) exhibit outstanding physical properties, including high thermal conductivity, excellent mechanical strength, and low electrical resistivity, which make them suitable candidates for a variety of applications. The work presented in this paper focuses on the pool boiling performance of refrigerant R-134a on microporous Cu-MWCNT composite surface layers. A two-stage electrodeposition technique was used to fabricate Cu-MWCNT composite coatings. In order to achieve variation in the surface properties of the Cu-MWCNT composite surface layer, electrodeposition was carried out at various bath temperatures (25 °C, 30 °C, 35 °C, and 40 °C). All surfaces coated with the Cu-MWCNT composite demonstrated superior boiling performance compared to the uncoated surface. Heat transfer coefficient (HTC) values for Cu-MWCNT composite surface layers, prepared at bath temperatures of 25 °C, 30 °C, 35 °C, and 40 °C, exhibited improvements of up to 1.75, 1.88, 2.06, and 2.22, respectively, in comparison to the plain Cu surface.

Keywords: HTC; pool boiling; electrodeposition; MWCNTs; R-134a



Citation: Pingale, A.D.; Katarkar, A.S.; Madgule, M.; Bhaumik, S.; Belgamwar, S.U. An Experimental Investigation on the Pool Boiling Heat Transfer of R-134a on Microporous Cu-MWCNT Composite Surfaces. *Thermo* **2024**, *4*, 16–28. <https://doi.org/10.3390/thermo4010002>

Academic Editor: Ignazio Blanco

Received: 15 December 2023

Revised: 6 January 2024

Accepted: 15 January 2024

Published: 17 January 2024



Copyright: © 2024 by the authors. Licensee MDPI, Basel, Switzerland. This article is an open access article distributed under the terms and conditions of the Creative Commons Attribution (CC BY) license (<https://creativecommons.org/licenses/by/4.0/>).

1. Introduction

In the past few decades, awareness about the importance of reducing energy use and protecting the environment has increased in response to the greenhouse effect generated by the burning of fossil fuels [1,2]. The Intergovernmental Panel on Climate Change's (IPCC) sixth assessment report emphasizes the urgency of taking action to reduce greenhouse gas emissions and limit global warming [3]. Greenhouse warming can be reduced by improving the efficiency of energy conversion devices. To achieve this objective, the performance of heat transfer in air-conditioning and refrigeration equipment has to be increased. Because of the high heat removal capacity, boiling heat transfer (BHT) has been used in several thermal management systems [4]. Recently, BHT has been proposed as a solution for systems with extremely high heat flux in a very compact volume. Therefore, boiling heat dissipation is extensively employed in various industrial sectors, including batteries for electric vehicles, electronic gadgets, boilers, nuclear power plants, and reactors [5].

In recent years, there has been a significant amount of research on methods for improving passive pool BHT with microscale surface cavities, porous coatings, and the growth of dendrite structures [6]. Active cavities are those cavities containing trapped non-condensable gases that usually generate bubbles [7]. A microporous coating is one of the best ways to improve pool BHT because it has more active cavities on the heating surface [8]. Microporous surfaces have been extensively researched in the literature. Anderson et al. [9] fabricated a microporous surface by vapor blasting on the Cu test surface, yielding a 170% increase in critical heat flux (CHF) with FC-87. Bergles et al. [10] used a proprietary method to fabricate porous surfaces on the bronze substrate, yielding 250%

enhancement in heat transfer coefficient (HTC) with water and up to 8 times enhancement with refrigerants. Sugiyama et al. [11] examined the pool BHT performance of R-114 on various surfaces. They discovered that the augmentation with porous heat transfer surface was only significant at low values of heat flux.

Numerous techniques, such as spray coating [12], RF sputtering [13], electrodeposition [14], PVD [15], e-beam evaporation [16], CVD [17], and dip coating [18], have been used to fabricate microporous coatings. Electrodeposition is preferred over available techniques for the preparation of microporous coatings on metallic heating surfaces because of its simplicity, controllability, and cost-effectiveness [19,20]. Gheitaghy et al. [21] systematically studied nanostructured microporous surfaces fabricated by electrodeposition techniques by varying electrolyte temperatures. Results showed that the HTC of the nanostructured microporous surface was 270% higher than that of the bare copper surface. Gupta et al. [22] prepared Cu-TiO₂ nanocomposite coatings by a two-step electrodeposition method. They found a significant augmentation of 185% in HTC and an increase of 86% in CHF compared with the bare copper surface. Protich et al. [23] developed a copper-graphene composite using an electrodeposition technique and reported augmentation of 66% in CHF. Katarkar et al. [19] fabricated microporous Cu-graphene composite coatings and attained a 97% increase in HTC relative to the bare Cu surface. Shakeri et al. [24] created hierarchical pattern heating surfaces using a combination of six-stage electrodeposition and photolithography techniques and achieved an improvement of about 119% in HTC compared to the bare surface. During electrodeposition, the surface roughness and porosity of copper coating can be tailored by varying the process parameters such as temperature, pH, current density, and rate of magnetic stirring [25]. In order to further enhance the pool BHT, the reinforcement of graphene oxide [26], graphene nanoplatelet [19], aluminum oxide [27], and titanium oxide [22] particles into copper matrix coatings have been used. Multiwalled carbon nanotubes (MWCNTs), a member of the carbon group, have extraordinary mechanical, thermal, thermodynamic, and electrochemical properties [28]. This study presents a microporous Cu-MWCNT composite heating surface that synergistically combines the high thermal conductivity of copper with the unique properties of MWCNTs. The reinforcement of MWCNTs into the copper matrix may help in enhancing the pool BHT performance. This advancement could revolutionize fields like electronics cooling, power generation, and thermal management in demanding industrial processes. However, the pool BHT performance on two-stage electro-co-deposited Cu-MWCNT composite coatings with R-134a is not studied yet.

In this research, MWCNT-reinforced Cu matrix (Cu-MWCNT) composite coatings were fabricated by varying bath temperatures (25 °C, 30 °C, 35 °C, and 40 °C) using a two-stage electrodeposition technique, and the pool BHT performance of R-134a on coated surfaces was examined. The effect of bath temperature on surface morphology, elemental composition, roughness, porosity, and wettability of Cu-MWCNT composite coatings was investigated. The microporous Cu-MWCNT composite-coated surfaces are prepared with the aim of reducing the energy loss from thermal systems and demonstrating their suitability for energy-saving applications.

2. Surface Preparation and Characterization

2.1. Materials

Copper sulfate pentahydrate (CuSO₄·5H₂O) and sulfuric acid (H₂SO₄) were obtained from Merck Life Science, Bengaluru, India. The MWCNTs (length = 1–10 μm, inner diameter = 2–6 nm, outer diameter = 10–15 nm, and purity = 90%) were received from Sigma-Aldrich, Bengaluru, India.

2.2. Two-Stage Electrodeposition

The copper substrates were ground with 120-, 400-, 800-, 1200-, and 2000-grade water-proof abrasive paper, and subsequently, cleaning was carried out using acetone to remove oil and similar dirt. After that, the copper substrates were washed with deionized (DI)

water and dried. The obtained substrate was considered as an uncoated Cu heating surface (surface roughness = $0.08 \pm 0.02 \mu\text{m}$) and also used to deposit composite coatings in the present work. The Cu-MWCNTs electroplating solution consisted of 100 g/L $\text{CuSO}_4 \cdot 5\text{H}_2\text{O}$, 5–30 g/L H_2SO_4 , 50 mg/L MWCNTs, and 500 mL DI water. The details of the operating conditions employed for the two-stage electrodeposition process are listed in Table 1. The cleaned copper substrate with the dimension of $\text{Ø } 9.0 \text{ mm}$ was employed as a cathode, and a pure copper plate (99.95%) was utilized as an anode. Prior to the deposition process, the plating solution was stirred to disperse the MWCNTs in the plating solution using a magnetic stirrer at 300 rpm for 1 h. After this, ultrasonic oscillation (20 kHz, 500 W) was provided for 45 min to evenly disperse MWCNTs in the electrolyte bath. The pH value of the bath was adjusted to 2 by adding H_2SO_4 . The electrodeposition of Cu-MWCNT composite coatings was carried out at various electrolyte bath temperatures using a two-stage electrodeposition technique, as shown in Figure 1. The higher current density (0.2 A/cm^2) was applied in the first stage for 60 s to form a microporous coating, and subsequently, a low current density was used for 0.5 h to provide more strength to the microporous structure. The evaluation of hydrogen bubbles on the surface of the coating was clearly observed during the deposition process.

Table 1. Processing parameters employed during two-stage electrodeposition.

Process Parameters	Range
pH	2
Bath Temperature	25 °C, 30 °C, 35 °C, 40 °C,
Ultrasonic treatment	20 kHz, 500 W for 45 min
Magnetic stirring	300 rpm
Electrodeposition time	60 s (1st stage); 30 min (2nd stage)
Current density	0.2 A/cm ² (1st stage); 0.05 A/cm ² (2nd stage)

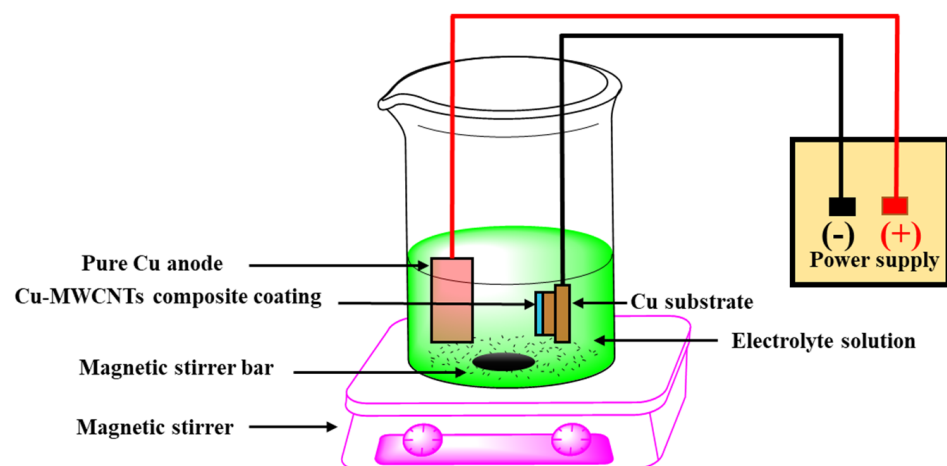


Figure 1. Schematic diagram of two-stage electrodeposition.

2.3. Characterization of Cu-MWCNT Composite Coatings

The morphologies and compositions of MWCNT and Cu-MWCNT composite coatings were examined by an FEI-Apreo-S scanning electron microscope with energy-dispersive spectroscopy (SEM/EDS, FEI, Delhi, India). The thicknesses of prepared coatings were gauged using a laser ellipsometer (Sentech, Mumbai, India). The roughness curve for Cu-MWCNT composite coatings was determined by a 2D profilometer (Taylor Habsons, Bengaluru, India). ImageJ software (1.54d) was employed to determine the porosity of the coating surface.

3. Experimental Setup and Procedure

3.1. Pool Boiling Experimental Setup

Figure 2 shows the essential components and apparatus used in the pool boiling experiments. The experimental setup consisted of a condensation unit, thermocouples, an electrical source, a copper block that served as the heater, and a cylindrical boiling vessel. The cylindrical boiling vessel (volume ≈ 4.48 L) was made of steel. It had two circular observation windows on either side, which were covered with Pyrex glass to allow for observation of the internal heating phenomenon. The vessel was sealed with two round steel flanges, one at the top and one at the bottom. A refrigerant injection device was mounted on the upper flange. The condensation coil condenses the evaporated vapor and helps to maintain the boiling vessel at the saturated level. The pressure of the heating vessel was monitored with a pressure gauge. The applied pressure of the saturation fluid was controlled by the electrical pressure limiter and controller, known as the pressure valve, within a specified pressure range. The boiling liquid in the pool was heated to a saturation temperature using a secondary heater. Appropriate exterior insulation made of glass fiber was used on the heating vessel to maintain isothermal conditions. To prevent heat from transferring from the copper blocks to the heating vessel, a Teflon ring was used to seal the joint between the bottom flanges of the heating vessel and the copper block. The cartridge heater was connected to a variac to control the heating power. The copper-heated blocks were placed over the lower portion of the test surface area. Three K-type thermocouples were inserted into the heating element at an angular distance of 120 degrees to monitor the temperature and heat flow of the test surface. To accurately measure the liquid's saturation temperature, another thermocouple was installed in the liquid.

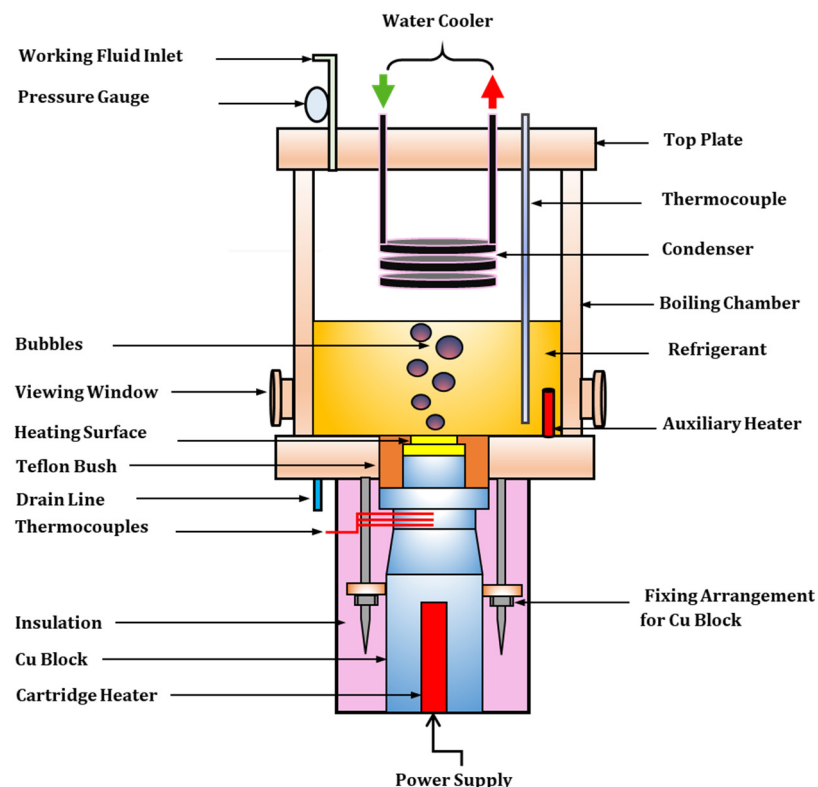


Figure 2. The schematic of pool boiling setup.

3.2. Experimental Procedure

Refrigerant R-134a was used to investigate the pool BHT of uncoated copper and coated Cu-MWCNT composite surface layers. The thermophysical fluid properties of R-134a are obtained from Ref. [29]. Acetone was used to rinse the heating boiling chamber

before each run of testing. The testing surface was mounted at the lower flange of the heating vessel. After installation, nitrogen gas was introduced into the vessel to check for leaks. Once the unit was confirmed to be leak-proof, R-134a coolant was added to the boiling vessel. The refrigerant R-134a was boiled for two hours using an additional heater to remove any dissolved gases. The pool BHT of R-134a was evaluated at a steady pressure ratio $\left(\frac{\text{Operating pressure}}{\text{Critical pressure}}\right)$ of 0.102 and an equilibrium temperature of 10 °C. During all the tests, the data points were taken in the order of increasing heat flux ranging from 7 to 60 kW/m² in the pool of 10 °C. The mass flow rate of the condensing liquid from the water chiller was adjusted for each power input to maintain a constant pressure in the system. The same experimental protocol was followed for each test surface. After each experiment, the test surface and coolant R-134a were removed from the boiling vessel.

4. Data Reduction and Uncertainty Analysis

4.1. Data Reduction

The schematic diagram of the heating section to measure the heat fluxes is shown in Figure 3a. In order to minimize heat losses in the radial direction and provision of 1D heat flow, the heating section was insulated with mineral insulation tape, polyethylene foam, and glass wool. To minimize the contact resistance, a thin layer of thermal grease was applied between the heating surface and the copper heating block. The entire assembly is then secured tightly inside a Teflon bush using a nut and bolt locking mechanism. Hence, in the present study, the contact resistance between the heating surface and the copper heating block is assumed to be neglected. The resistance diagram, shown in Figure 3b, was used to calculate the surface temperatures. Please note that Figure 3b is not drawn to scale. The rates of heat transfer (Q) in various sections (A), (B), (C), (D), and (E) were determined using Fourier's law of heat conduction equation along the axial direction of heating section, represented by Equations (1), (2), (3), (4) and (5), respectively.

$$Q_A = kA_A \frac{T_3 - T_4}{X_1} \quad (1)$$

$$Q_B = kA_B \frac{T_4 - T_5}{X_2} \quad (2)$$

$$Q_C = kA_C \frac{T_5 - T_6}{X_3} \quad (3)$$

$$Q_D = kA_D \frac{T_6 - T_7}{X_4} \quad (4)$$

$$Q_E = kA_E \frac{T_7 - T_S}{X_5} \quad (5)$$

where k is thermal conductivity, A is the area of the section, and X is the section length.

The surface temperature (T_S) was determined by Equation (6):

$$T_S = T_3 - \frac{VI}{k} \left(\frac{X_1}{A_A} + \frac{X_2}{A_B} + \frac{X_3}{A_C} + \frac{X_4}{A_D} + \frac{X_5}{A_E} \right) \quad (6)$$

Heat flux (q) was determined by Equation (7):

$$q = \frac{Q}{A_E} \quad (7)$$

The BHT coefficient can be obtained by Equation (8):

$$h = \frac{q}{T_S - T_{sat}} \quad (8)$$

where T_{sat} is the saturation temperature of the working fluid (R-134a).

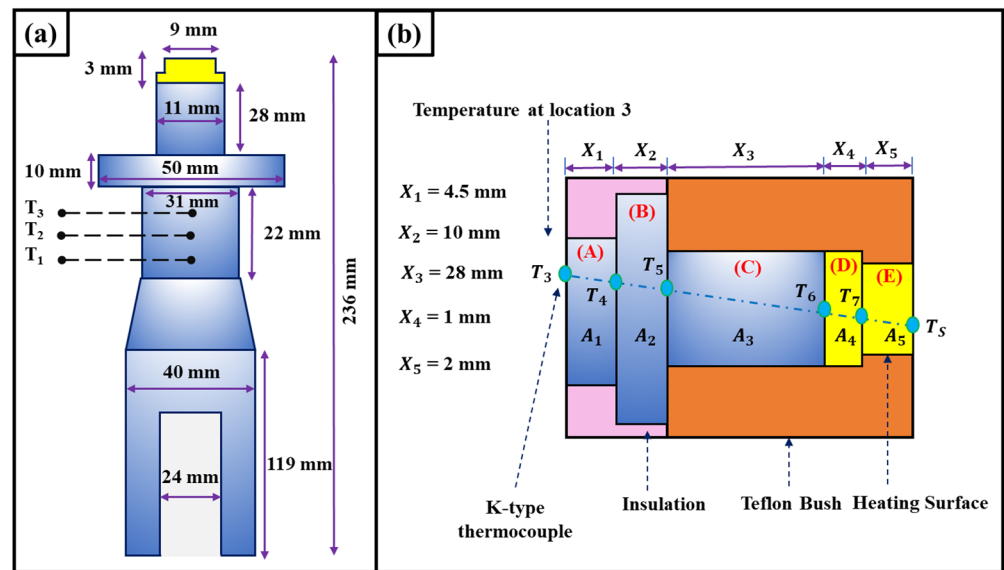


Figure 3. Schematic diagram of (a) heating section and (b) resistance diagram.

4.2. Uncertainty Analysis

Uncertainty analysis of the measuring devices and experimental data was performed using the methodology proposed by Schultz and Cole [30].

$$\text{Mathematically, } U_y = \left[\sum_{i=1}^n \left\{ \left(\frac{\partial y}{\partial x_i} \right) U_{x_i} \right\}^2 \right]^{\frac{1}{2}} \quad (9)$$

where U_{x_i} is uncertainty associated with x_i , and y is the calculated parameter.

The systematic errors for temperature, voltage, length, and current measurements were determined to be ± 0.1 °C, ± 0.01 V, ± 1.0 mm, and ± 0.002 A, respectively. The calculated uncertainties for wall superheat (ΔT), heat transfer coefficient (h), and heat flux (q) were $\pm 7.8\%$, $\pm 8.2\%$, and $\pm 3.2\%$, respectively.

5. Results and Discussion

5.1. Surface Characterization of Cu-MWCNT Composite Coatings

The FE-SEM images of the Cu-MWCNT composite surface layers deposited at various bath temperatures are depicted in Figure 4. At low bath temperatures (25 °C and 30 °C), the surface of the Cu-MWCNT composite appears relatively smooth, as seen in Figure 4a–d. With an increase in bath temperature (35 °C and 40 °C), the Cu-MWCNT composite coating grows relatively quickly, resulting in high surface roughness and larger particle size (see Figure 4e–h). The existence of micropores is clearly observed in Figure 4g,h. This is mainly due to the fast crystallization of the composite coating in a high-temperature environment. The EDS element distribution map and corresponding EDS spectrum of Cu-MWCNT composite coating deposited at 40 °C are shown in Figure 5a,b. As shown in Figure 5, Cu and C elements are uniformly distributed in the Cu-MWCNT composite coating, confirming the reinforcement of MWCNTs into the copper matrix. The effect of various bath temperatures on coating thickness and surface properties, such as surface roughness and porosity, is also studied. The porosity, surface roughness, and thickness of Cu-MWCNT composite coatings increase as the bath temperature increases (Table 2). This is mainly due to the rise in the deposition rate of Cu^{2+} with an increase in bath temperature from 25 °C to 40 °C. The maximum average surface roughness of 36 μm was obtained in the Cu-MWCNT composite coating at 40 °C, as shown in Figure 6.

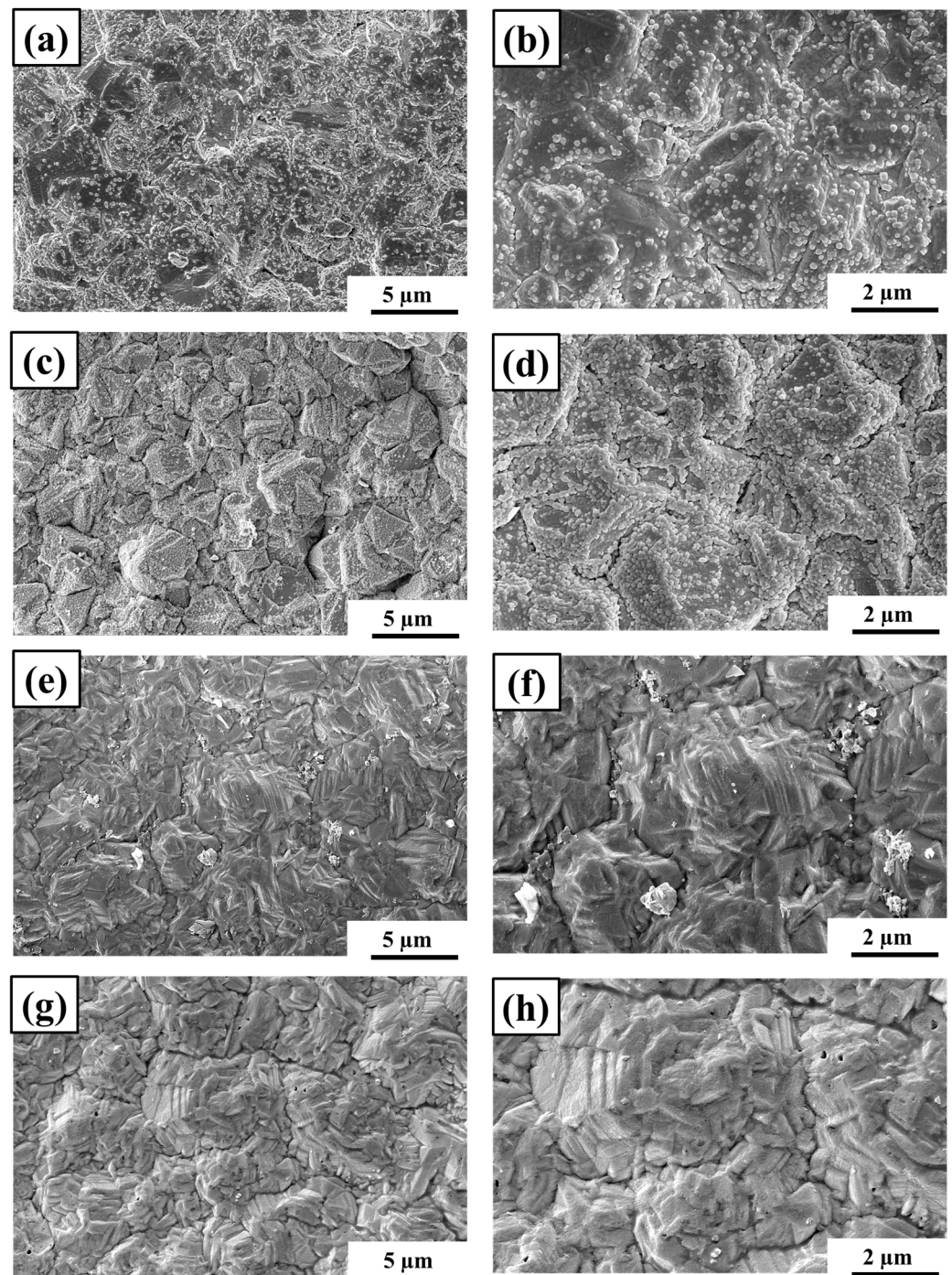


Figure 4. Surface characterization of deposited Cu-MWCNT composite coatings at different bath temperatures: (a,b) 25 °C; (c,d) 30 °C; (e,f) 35 °C; (g,h) 40 °C.

Table 2. Porosity, surface roughness, and thickness of Cu-MWCNT composite coatings.

Coating	Porosity (%)	Surface Roughness (μm)	Thickness (μm)
Cu-MWCNTs (25 °C)	32 ± 4	0.18 ± 0.04	14 ± 4
Cu-MWCNTs (30 °C)	38 ± 5	0.25 ± 0.04	18 ± 4
Cu-MWCNTs (35 °C)	44 ± 5	0.29 ± 0.05	23 ± 3
Cu-MWCNTs (40 °C)	49 ± 4	0.36 ± 0.06	27 ± 4

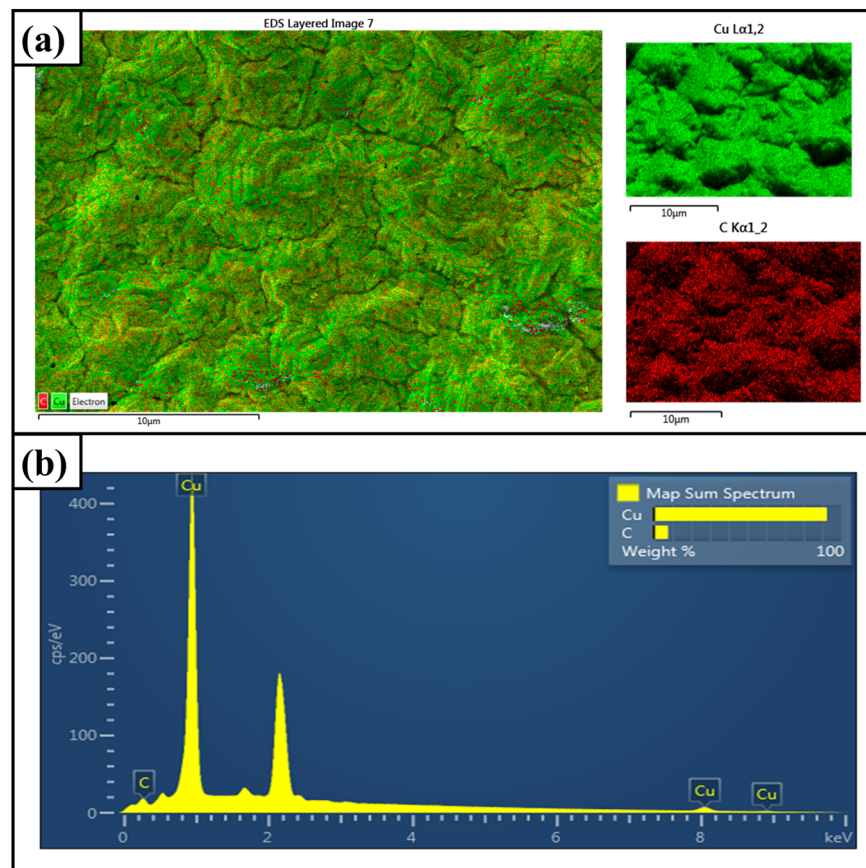


Figure 5. Characterization of Cu-MWCNT composite coating (40 °C). (a) EDS map. (b) Dispersion energy spectrum.

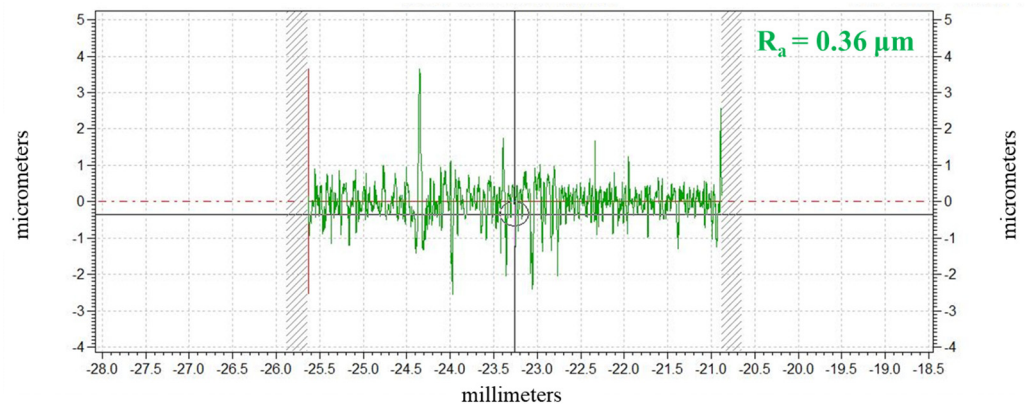


Figure 6. Roughness curve for Cu-MWCNT composite coating (40 °C).

5.2. Analysis of Pool Boiling Curves

Figure 7 illustrates the variations of the heat flux (q) in relation to the wall superheat (ΔT). The boiling heat transfer curves obtained in the current experimental setup for Cu-MWCNT composite surface layers prepared at different bath temperatures display various shapes, mainly due to the combination of heat transfer surface properties and the thermal properties of the boiling refrigerant. The Cu-MWCNT composite coating electrodeposited at a bath temperature of 40 °C exhibited a higher heat transfer rate than the uncoated Cu surface at the same value of wall superheat. With an increase in bath temperature from 25 °C to 40 °C, the Cu-MWCNT composite surface layer showed a further increase in the boiling performance. The Cu-MWCNT composite coating (40 °C) achieved a wall

superheat value of around 4.14 K. This wall superheat value was significantly lower than that of the plain Cu plate, which attained its wall superheat value of about 8.80 K. It was reported that heat transfer performance of microporous coated heat transfer surfaces was significantly affected by factors such as coating thickness, surface roughness, porosity, and the thermo-physical characteristics of the boiling fluid as evidence of previous work [31]. For R-134a, the Cu-MWCNT composite coating (40 °C) demonstrated the lowest wall superheat as compared to all other heating surfaces. This may be because of the larger heat transfer area and the presence of micropores on the surface Cu-MWCNT composite coating (see Figure 4g,h).

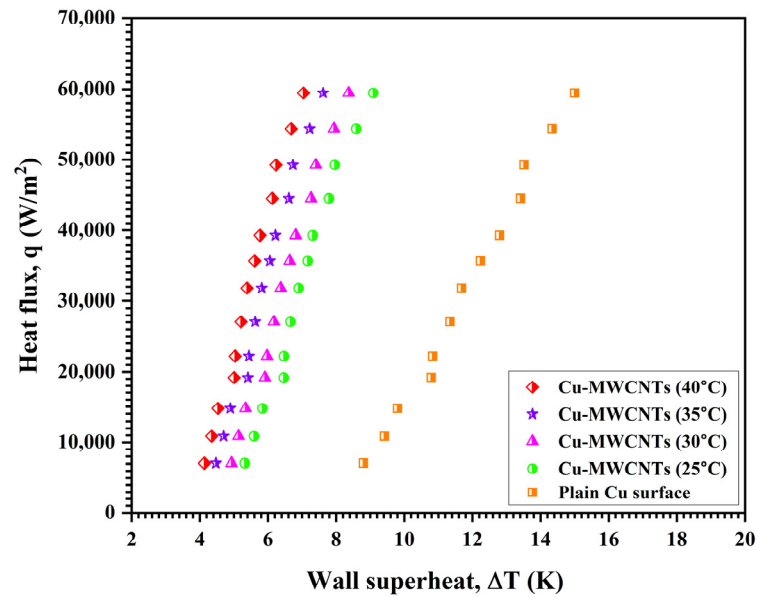


Figure 7. Heat flux vs. wall superheat.

The variation of the heat transfer coefficient (h) with respect to heat flux (q) for Cu-MWCNT composite surface layers prepared at different bath temperatures is represented in Figure 8. Compared with the bare Cu heating surface, the Cu-MWCNT composite coatings electrodeposited at different bath temperatures had significantly higher values of the heat transfer coefficient at the same values of heat flux. The Cu-MWCNT composite coating (40 °C) achieved the highest heat transfer coefficient of approximately 8.44 kW/m²·K at a heat flux of 59.46 kW/m², with a significantly lower wall superheat value (around 7.04 K) compared to the plain Cu plate. The plain Cu plate attained its higher heat flux of 3.96 kW/m²·K at the same heat flux value but with a much higher wall superheat value (around 15 K). The enhanced performance can be attributed to two main factors: the increased heat transfer area of the two-stage electrodeposited composite surfaces and the presence of microporosity. This microporosity facilitates the flow of refrigerant toward the heating surface and the escape of vapor from the coated surface by providing a network of interconnected void spaces.

Figure 9 illustrates the variation in the enhancement ratio ($h_{ER} = \frac{h_{coated}}{h_{uncoated}}$) as a function of heat flux. It can be seen from Figure 9 that the maximum h_{ER} values for Cu-MWCNT composite coatings electrodeposited at bath temperatures of 25 °C, 30 °C, 35 °C, and 40 °C are 1.75, 1.88, 2.06, and 2.22, respectively, over the bare Cu surface. However, for composite-coated surfaces, the values of the highest h_{ER} were achieved before the test maximum heat flux was reached.

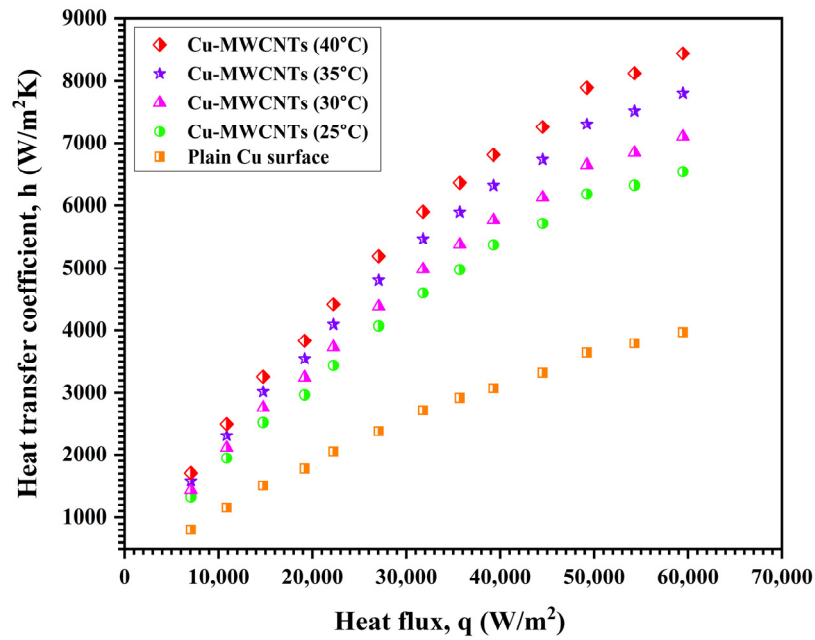


Figure 8. Variation of heat transfer coefficient with heat flux.

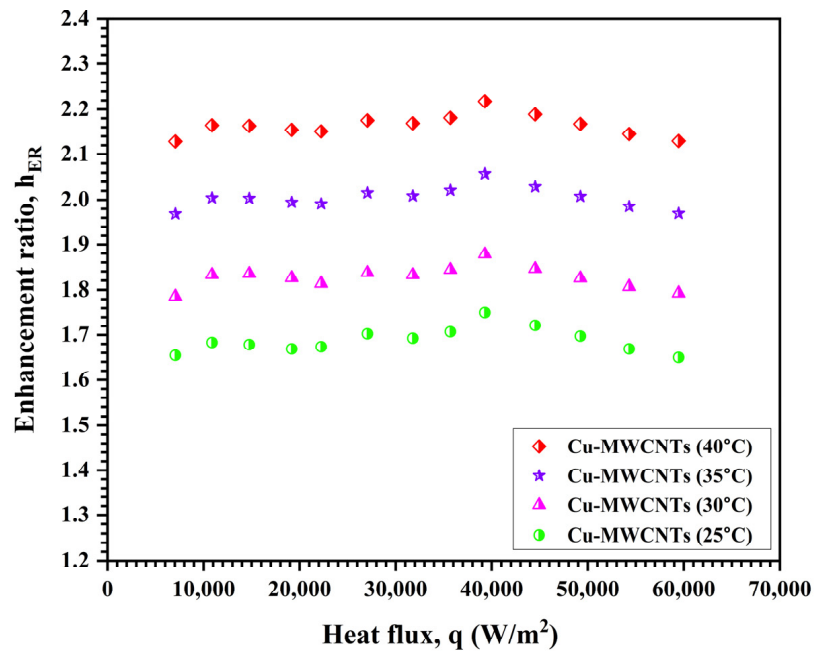


Figure 9. Enhancement ratio vs. heat flux.

5.3. Comparison of the Present Work with Previous Ones

The comparison of the present work with other previously reported microporous heating surfaces in terms of HTC improvement is listed in Table 3. As observed from Table 3, the experimental results for the prepared Cu-MWCNT composite surface layers were similar to or better than the results for the other heating surfaces. This comparison reveals that the Cu-MWCNT composite surface layer fabricated by the two-stage electrodeposition technique is particularly well suited for real-world boiling heat transfer applications owing to the increased nucleation site density, a larger surface area, and increased capillary-assisted liquid supply.

Table 3. Comparative assessment of this work with published literature.

Coating	Base Material	Working Fluid	Coating Method	Remark	Ref.
Cu-MWCNTs	Cu	R-134a	Two-step electrodeposition	HTC increased by 122%	Present work
Al@GNPs	Al	R-134a	Mechanical milling, screen printing, and sintering	HTC increased by 143%	[32]
Graphene/CNT	Cu	DI water	Self-assembling	HTC increased by 100%	[33]
Cu-GNPs	Cu	R-134a	Two-step electrodeposition	HTC increased by 97%	[19]
GO	Cu	DI water	Dip coating	HTC increased by 47%	[34]
CNT-Cu	Cu	R-134a	Mechanical alloying and cold spray	HTC increased by 74%	[35]
Cu and graphene	Cu	DI water	Electrodeposition and dip coating	HTC increased by 82%	[36]
Cu-Zinc	Cu	HFE-7200	Electrophoretic deposition	HTC increased by 100%	[37]
Al ₂ O ₃	Cu	SES36	Electrophoretic deposition	HTC increased by 76.9%	[38]
TiO ₂	Cu	R134a	Electron beam evaporation	HTC increased by 87.5%	[39]
Cu particles	Cu	R-134a	Powder flame spraying	HTC increased by 100%	[40]

6. Conclusions

In summary, a Cu-MWCNT composite coating was synthesized by a two-stage electrodeposition technique at various bath temperatures. Serving as the heating surface, the Cu-MWCNT composite surface layer has significantly enhanced the pool BHT of R-134a. The Cu-MWCNT composite coating fabricated at a bath temperature of 40 °C showed the highest surface porosity of 49%, a coating thickness of 27 µm, and a surface roughness of 36 µm among all the prepared coatings. Results demonstrated that modified surfaces fabricated using the two-stage electrodeposition technique exhibit enhanced surface properties, leading to an increased nucleation site density. Compared to the uncoated Cu surface, the wall superheat for the Cu-MWCNT composite surface layer (40 °C) was reduced by 53%. The highest h_{ER} values for the Cu-MWCNT composite surface layer electrodeposited at 25 °C, 30 °C, 35 °C, and 40 °C were found to be 1.75, 1.88, 2.06, and 2.22, respectively, over bare Cu surface. Overall, the thicker Cu-MWCNT composite surface layer (40 °C) is a more effective heat transfer material than the thinner coatings. This is due to its larger heat transfer area and higher nucleation site density.

Author Contributions: Conceptualization, A.D.P., A.S.K. and M.M.; methodology, A.D.P., A.S.K. and M.M.; software, A.D.P., A.S.K. and M.M.; validation, A.D.P., A.S.K. and M.M.; formal analysis, A.D.P., A.S.K. and M.M.; investigation, A.D.P., A.S.K. and M.M.; resources, S.U.B. and S.B.; data curation, A.D.P., A.S.K. and M.M.; writing—original draft preparation, A.D.P., A.S.K. and M.M.; writing—review and editing, A.D.P., A.S.K., M.M., S.U.B. and S.B.; supervision, S.U.B. and S.B.; project administration, A.D.P., A.S.K., M.M., S.U.B. and S.B. All authors have read and agreed to the published version of the manuscript.

Funding: This research received no external funding.

Data Availability Statement: The data generated during and/or analyzed during the current study are available from the corresponding author upon reasonable request.

Conflicts of Interest: The authors declare no conflicts of interest.

References

- Dey, S.; Sreenivasulu, A.; Veerendra, G.T.N.; Rao, K.V.; Babu, P.S.S.A. Renewable Energy Present Status and Future Potentials in India: An Overview. *Innov. Green Dev.* **2022**, *1*, 100006. [[CrossRef](#)]
- Perkins, O.; Alexander, P.; Arneeth, A.; Brown, C.; Millington, J.D.A.; Rounsevell, M. Toward Quantification of the Feasible Potential of Land-Based Carbon Dioxide Removal. *One Earth* **2023**, *6*, 1638–1651. [[CrossRef](#)]

3. Calvin, K.; Dasgupta, D.; Krinner, G.; Mukherji, A.; Thorne, P.W.; Trisos, C.; Romero, J.; Aldunce, P.; Barrett, K.; Blanco, G.; et al. *IPCC, 2023: Climate Change 2023: Synthesis Report. Contribution of Working Groups I, II and III to the Sixth Assessment Report of the Intergovernmental Panel on Climate Change*; Core Writing Team, Lee, H., Romero, J., Eds.; IPCC: Geneva, Switzerland, 2023. [[CrossRef](#)]
4. Petrovic, M.M.; Stevanovic, V.D. Pool Boiling Simulation with Two-Fluid and Grid Resolved Wall Boiling Model. *Int. J. Multiph. Flow* **2021**, *144*, 103806. [[CrossRef](#)]
5. Liu, B.; Yang, X.; Li, Q.; Chang, H.; Qiu, Y. Enhanced Pool Boiling on Composite Microstructured Surfaces with Microcavities on Micro-Pin-Fins. *Int. Commun. Heat Mass Transf.* **2022**, *138*, 106350. [[CrossRef](#)]
6. Rainey, K.; You, S.; Lee, S. Effect of Pressure, Subcooling, and Dissolved Gas on Pool Boiling Heat Transfer from Microporous, Square Pin-Finned Surfaces in FC-72. *Int. J. Heat Mass Transf.* **2003**, *46*, 23–35. [[CrossRef](#)]
7. Mudhafar, M.A.H.; Zheng-hao, W. Optimization of Pool Boiling Heat Transfer on Microporous Metal Coating Surfaces with FC-72 as a Working Fluid. *Heat Mass Transf.* **2022**, *58*, 1963–1977. [[CrossRef](#)]
8. Jun, S.; Kim, J.; Son, D.; Kim, H.Y.; You, S.M. Enhancement of Pool Boiling Heat Transfer in Water Using Sintered Copper Microporous Coatings. *Nucl. Eng. Technol.* **2016**, *48*, 932–940. [[CrossRef](#)]
9. Anderson, T.M.; Mudawar, I. Microelectronic Cooling by Enhanced Pool Boiling of a Dielectric Fluorocarbon Liquid. *J. Heat Transf.* **1989**, *111*, 752–759. [[CrossRef](#)]
10. Bergles, A.E.; Chyu, M.C. Characteristics of Nucleate Pool Boiling from Porous Metallic Coatings. *J. Heat Transf.* **1982**, *104*, 279–285. [[CrossRef](#)]
11. Memory, S.B.; Sugiyama, D.C.; Marto, P.J. Nucleate Pool Boiling of R-114 and R-114-Oil Mixtures from Smooth and Enhanced Surfaces—I. Single Tubes. *Int. J. Heat Mass Transf.* **1995**, *38*, 1347–1361. [[CrossRef](#)]
12. Ahmad, S.W.; Lewis, J.S.; McGlen, R.J.; Karayiannis, T.G. Pool Boiling on Modified Surfaces Using R-123. *Heat Transf. Eng.* **2014**, *35*, 1491–1503. [[CrossRef](#)]
13. Saha, B.; Das, N.S.; Chattopadhyay, K.K. Combined Effect of Oxygen Deficient Point Defects and Ni Doping in Radio Frequency Magnetron Sputtering Deposited ZnO Thin Films. *Thin Solid Films* **2014**, *562*, 37–42. [[CrossRef](#)]
14. Patil, C.M.; Santhanam, K.S.V.; Kandlikar, S.G. Development of a Two-Step Electrodeposition Process for Enhancing Pool Boiling. *Int. J. Heat Mass Transf.* **2014**, *79*, 989–1001. [[CrossRef](#)]
15. Karunakaran, B.; Rajendra Kumar, R.T.; Senthil Kumar, V.; Mangalaraj, D.; Narayandass, S.K.; Mohan Rao, G. Structural Characterization of DC Magnetron-Sputtered TiO₂ Thin Films Using XRD and Raman Scattering Studies. *Mater. Sci. Semicond. Process.* **2003**, *6*, 547–550. [[CrossRef](#)]
16. Ray, M.; Bhaumik, S. Structural Properties of Glancing Angle Deposited Nanostructured Surfaces for Enhanced Boiling Heat Transfer Using Refrigerant R-141b. *Int. J. Refrig.* **2018**, *88*, 78–90. [[CrossRef](#)]
17. Ujereh, S.; Fisher, T.; Mudawar, I. Effects of Carbon Nanotube Arrays on Nucleate Pool Boiling. *Int. J. Heat Mass Transf.* **2007**, *50*, 4023–4038. [[CrossRef](#)]
18. Lee, J.; Son, G. Numerical Simulation of Liquid Film Formation and Evaporation in Dip Coating. *Int. Commun. Heat Mass Transf.* **2015**, *68*, 220–227. [[CrossRef](#)]
19. Katarkar, A.S.; Pingale, A.D.; Belgamwar, S.U.; Bhaumik, S. Experimental Study of Pool Boiling Enhancement Using a Two-Step Electrodeposited Cu–GNPs Nanocomposite Porous Surface with R-134a. *J. Heat Transfer* **2021**, *143*, 121601. [[CrossRef](#)]
20. Rishi, A.M.; Kandlikar, S.G.; Gupta, A. Improved Wettability of Graphene Nanoplatelets (GNP)/Copper Porous Coatings for Dramatic Improvements in Pool Boiling Heat Transfer. *Int. J. Heat Mass Transf.* **2019**, *132*, 462–472. [[CrossRef](#)]
21. Gheitaighy, A.M.; Saffari, H.; Zhang, G.Q. Effect of Nanostructured Microporous Surfaces on Pool Boiling Augmentation. *Heat Transf. Eng.* **2019**, *40*, 762–771. [[CrossRef](#)]
22. Gupta, S.K.; Misra, R.D. Effect of Two-Step Electrodeposited Cu–TiO₂ Nanocomposite Coating on Pool Boiling Heat Transfer Performance. *J. Therm. Anal. Calorim.* **2019**, *136*, 1781–1793. [[CrossRef](#)]
23. Protich, Z.; Santhanam, K.S.V.; Jaikumar, A.; Kandlikar, S.G.; Wong, P. Electrochemical Deposition of Copper in Graphene Quantum Dot Bath: Pool Boiling Enhancement. *J. Electrochem. Soc.* **2016**, *163*, E166–E172. [[CrossRef](#)]
24. Shakeri, H.; Moghadasi, H.; Saffari, H. Experimental Parametric Study of Hierarchical Micro/Nano Electrodeposited (Six-Step) Pattern with Respect to Volcano-Shape Morphology in Pool Boiling Performance Augmentation. *Exp. Heat Transf.* **2021**, *36*, 210–233. [[CrossRef](#)]
25. Katarkar, A.S.; Pingale, A.D.; Belgamwar, S.U.; Bhaumik, S. Experimental Investigation of Pool Boiling Heat Transfer Performance of Refrigerant R-134a on Differently Roughened Copper Surfaces. *Mater. Today Proc.* **2021**, *47*, 3269–3275. [[CrossRef](#)]
26. Rishi, A.M.; Kandlikar, S.G.; Gupta, A. Repetitive Pool Boiling Runs: A Controlled Process to Form Reduced Graphene Oxide Surfaces from Graphene Oxide with Tunable Surface Chemistry and Morphology. *Ind. Eng. Chem. Res.* **2019**, *58*, 7156–7165. [[CrossRef](#)]
27. Gupta, S.K.; Misra, R.D. Experimental Study of Pool Boiling Heat Transfer on Copper Surfaces with Cu–Al₂O₃ Nanocomposite Coatings. *Int. Commun. Heat Mass Transf.* **2018**, *97*, 47–55. [[CrossRef](#)]
28. Alshahrani, A.A.; Al-Zoubi, H.; Alotaibi, S.E.; Hassan, H.M.A.; Alsohaimi, I.H.; Alotaibi, K.M.; Alshammari, M.S.; Nghiem, L.; Panhuis, M. in het Assessment of Commercialized Nylon Membranes Integrated with Thin Layer of MWCNTs for Potential Use in Desalination Process. *J. Mater. Res. Technol.* **2022**, *21*, 872–883. [[CrossRef](#)]

29. Katarkar, A.S.; Pingale, A.D.; Belgamwar, S.U.; Bhaumik, S. Fabrication of Cu@G Composite Coatings and Their Pool Boiling Performance with R-134a and R-1234yf. *Adv. Mater. Process. Technol.* **2022**, *8*, 2044–2056. [[CrossRef](#)]
30. Schultz, R.R.; Cole, R. Uncertainty Analysis of Boiling Nucleation. In Proceedings of the AIChE symposium series, Los Angeles, CA, USA, 16–21 November 1997; AIChE: New York, NY, USA, 1979; Volume 75, pp. 32–38.
31. Demiray, F.; Kim, J. Heat Transfer from a Single Bubble Nucleation Site during Saturated Pool Boiling of FC-72 Using an Array of 100 Micron Heaters. In Proceedings of the 8th AIAA/ASME Joint Thermophysics and Heat Transfer Conference, St. Louis, MI, USA, 24–26 June 2002; American Institute of Aeronautics and Astronautics: Reston, VA, USA, 2002.
32. Majumder, B.; Pingale, A.D.; Katarkar, A.S.; Belgamwar, S.U.; Bhaumik, S. Enhancement of Pool Boiling Heat Transfer Performance of R-134a on Microporous Al@GNPs Composite Coatings. *Int. J. Thermophys.* **2022**, *43*, 49. [[CrossRef](#)]
33. Sezer, N.; Khan, S.A.; Koç, M. Amelioration of the Pool Boiling Heat Transfer Performance via Self-Assembling of 3D Porous Graphene/Carbon Nanotube Hybrid Film over the Heating Surface. *Int. J. Heat Mass Transf.* **2019**, *145*, 118732. [[CrossRef](#)]
34. Jaikumar, A.; Kandlikar, S.G.; Gupta, A. Pool Boiling Enhancement through Graphene and Graphene Oxide Coatings. *Heat Transf. Eng.* **2017**, *38*, 1274–1284. [[CrossRef](#)]
35. Pialago, E.J.T.; Kwon, O.K.; Park, C.W. Nucleate Boiling Heat Transfer of R134a on Cold Sprayed CNT–Cu Composite Coatings. *Appl. Therm. Eng.* **2013**, *56*, 112–119. [[CrossRef](#)]
36. Jaikumar, A.; Santhanam, K.S.V.; Kandlikar, S.G.; Raya, I.B.P.; Raghupathi, P. Electrochemical Deposition of Copper on Graphene with High Heat Transfer Coefficient. *ECS Trans.* **2015**, *66*, 55–64. [[CrossRef](#)]
37. Cao, Z.; Wu, Z.; Abbood, S.; Sundén, B. An Analysis of Pool Boiling Heat Transfer on Nanoparticle-Coated Surfaces. *Energy Procedia* **2019**, *158*, 5880–5887. [[CrossRef](#)]
38. Song, G.; Davies, P.A.; Wen, J.; Xu, G.; Quan, Y. Nucleate Pool Boiling Heat Transfer of SES36 Fluid on Nanoporous Surfaces Obtained by Electrophoretic Deposition of Al₂O₃. *Appl. Therm. Eng.* **2018**, *141*, 143–152. [[CrossRef](#)]
39. Ray, M.; Bhaumik, S. Nucleate Pool Boiling Heat Transfer of Hydro-Fluorocarbon Refrigerant R134a on TiO₂ Nanoparticle Coated Copper Heating Surfaces. *Heat Transf. Eng.* **2019**, *40*, 997–1006. [[CrossRef](#)]
40. Dewangan, A.K.; Kumar, A.; Kumar, R. Experimental Study of Nucleate Pool Boiling of R-134a and R-410a on a Porous Surface. *Heat Transf. Eng.* **2019**, *40*, 1249–1258. [[CrossRef](#)]

Disclaimer/Publisher’s Note: The statements, opinions and data contained in all publications are solely those of the individual author(s) and contributor(s) and not of MDPI and/or the editor(s). MDPI and/or the editor(s) disclaim responsibility for any injury to people or property resulting from any ideas, methods, instructions or products referred to in the content.